SoC-Based Dynamic Power Sharing Method with AC-Bus Voltage Restoration for Microgrid Applications

Lu, Xiaonan; Sun, Kai; Guerrero, Josep M.; Huang, Lipei

Published in:
Proceedings of the 38th Annual Conference of the IEEE Industrial Electronics Society

DOI (link to publication from Publisher):
10.1109/IECON.2012.6389058

Publication date:
2012

Document Version
Early version, also known as pre-print

This document is a preprint of the final paper: *Lu, Xiaonan; Sun, Kai; Guerrero, Josep; Huang, Lipei; , "SoC-based dynamic power sharing method with AC-bus voltage restoration for microgrid applications," IECON 2012 - 38th Annual Conference on IEEE Industrial Electronics Society , vol., no., pp.5677-5682, 25-28 Oct. 2012. doi: 10.1109/IECON.2012.6389058*
URL: http://ieeexplore.ieee.org/stamp/stamp.jsp?tp=&arnumber=6389058&isnumber=6388505

SoC-Based Dynamic Power Sharing Method with AC-Bus Voltage Restoration for Microgrid Applications

Xiaonan Lu[1] Kai Sun[1] Josep Guerrero[2, 3] Lipei Huang[1]
1. State Key Lab of Power Systems, Department of Electrical Engineering, Tsinghua University, Beijing, China
2. Department of Energy Technology, Aalborg University, Aalborg, Denmark, email: joz@et.aau.dk

***Abstract* – In a microgrid system, the distributed energy storage units are commonly employed as the energy buffer. In this paper, a dynamic power sharing method based on the state-of-charge (SoC) of each energy storage unit is proposed. Droop control is employed as the basic control strategy for the distributed energy storage units. By using the proposed method, the coefficients in the conventional droop method are adjusted according to the SoC of each energy storage module. The modules with higher SoC will generate more active power, while those with lower SoC will generate less. Meanwhile, the reactive power is equally shared in the energy storage system. The relationship between the droop coefficient and SoC are studied deeply and the small signal model is developed to verify the stability of the control system. It is found that the active power sharing speed becomes faster with higher power exponent of SoC. At the same time, in order to restore the AC-bus voltage, secondary control is employed to eliminate the deviations of the frequency and amplitude caused by the droop control, with the droop coefficients adjusting according to the SoCs. The model of the secondary control scheme for SoC-based droop method is developed and its stability is discussed. The theoretical analysis is demonstrated by both simulation and experimental results.**

I. INTRODUCTION

Considering the growing energy needs and existing problems of conventional fossil fuel, renewable energy has been highly penetrated into the modern electrical grid nowadays. In order to integrate different kinds of renewable energy sources into one area, the concept of microgrid was proposed several years ago [1]. In a microgrid, the distributed sources are usually connected to the point of common coupling (PCC) by the power electronics interfaces [2]. According to the feature of distributed structure, the interface converters are commonly connected in parallel. Control of these parallel interface converters is a key problem in microgrid applications [3]. The most significant issue in the parallel converter control is the load power sharing. In order to achieve this target, several control methods are proposed by researchers. Some of them are based on high frequency communication [4], which is not suitable for the distributed connection in a microgrid system. Droop control is involved in the inverter-interfaced distributed system, for no communication or only low bandwidth communication is required [3-5]. Without the high frequency communication, the overall system cost is reduced and the reliability of the system is enhanced.

For the uncertainty property of the renewable energy sources, the energy storage units are commonly employed as the energy buffers [6]. Since the State-of-Charge (SoC) of each energy storage unit is changing during its usage, the output power of each unit should be adjusted accordingly. The unit with higher SoC should provide more power, while the one with lower SoC should provide less. Hence, to take the distributed feature and SoC together into account, SoC-based droop method is employed, which works like gain-scheduling droop control [7-8]. In the existing research work, the droop coefficient of each interface converter is commonly in inverse proportion to the SoC of the connected energy storage. Actually, different relationships between the droop coefficient and SoC can be further studied to reach the desired dynamic power sharing performance.

Though droop control method has several advantages, its drawback should be noticed. In the droop-controlled parallel inverter system, PCC voltage deviation happens [3, 5]. Therefore, the voltage performance is degraded, which may influence the operation of the loads connected to the common buses. To deal with the above problem, the droop coefficient should be designed to guarantee that the deviation will not exceed the acceptable range. Meanwhile, the secondary control based on the low-bandwidth communication is proposed to restore the common bus voltage [5]. Conventionally, the secondary control is employed in the droop-controlled system with constant droop coefficients. In the application of SoC-based droop method, as the droop coefficients are changing according to the SoC, the performance of secondary control and the overall system stability should be further studied.

In this paper, SoC-based droop control method is employed to reach dynamic power sharing in an AC microgrid. Different kinds of relationships between the droop coefficient and SoC are discussed to improve the dynamic sharing performance. Secondary control scheme with variable droop coefficients is also employed to restore the frequency and amplitude of the AC-bus voltage. Modeling of the overall control system including both SoC-based droop control and secondary control are established, based on which the system stability is tested. The theoretical analysis is demonstrated by both simulation and experimental results.

II. MODEL OF THE CONTROL SYSTEM

A. SoC-*based droop control method*

The power electronics interface inverters are commonly connected in parallel in a microgrid, as shown in Fig. 1. If the inductive output impedance is guaranteed in the system, the conventional droop control method in an AC microgrid is shown as

$$f = f^* - m \cdot p_{\text{AC LPF}} \tag{1}$$

$$E = E^* - n \cdot q_{\text{AC LPF}} \tag{2}$$

where f and E are the frequency and amplitude of the local AC output voltage, $p_{\text{AC LPF}}$ and $q_{\text{AC LPF}}$ are the filtered active and reactive in the AC side, m and n are the droop coefficients.

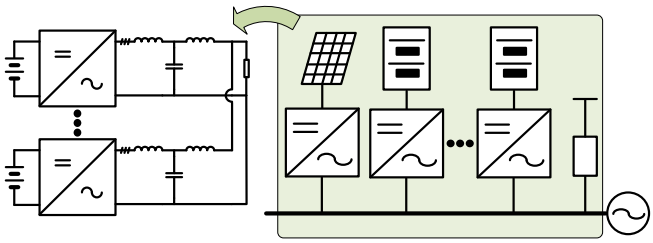

Fig. 1. Parallel interface inverters in an AC microgrid.

When the DC sides of the parallel inverters are connected to the distributed energy storage modules, it is necessary to share the active power according to the SoC of each unit. Concretely, the energy storage unit with higher SoC should generate more active power, while the one with lower SoC should generate less. In the control system of this paper, the SoC is calculated by coulomb counting, as shown below.

$$SoC_1 = SoC_1^* - \frac{1}{C_e}\int i_{\text{DC1}} dt \tag{3}$$

$$SoC_2 = SoC_2^* - \frac{1}{C_e}\int i_{\text{DC2}} dt \tag{4}$$

where SoC_1^* and SoC_2^* are the initial value of the SoCs, i_{DC1} and i_{DC2} are the output current of each energy storage unit, C_e is the capacity.

Ignoring the power loss in the interface inverter, it yields that

$$p_{\text{AC1}} = p_{\text{in1}} = v_{\text{DC1}} i_{\text{DC1}} \tag{5}$$

$$p_{\text{AC2}} = p_{\text{in2}} = v_{\text{DC2}} i_{\text{DC2}} \tag{6}$$

where p_{AC1} and p_{AC2} are the AC output power, p_{in1} and p_{in2} are the input power, v_{DC1} and v_{DC2} are the DC voltage.

For SoC changes very slow and the output voltage of each energy storage unit stays constant in a large range of SoC, it can be supposed that the output voltage of each unit keeps constant. Meanwhile, if different energy storage units are in the same voltage level, it is obtained that

$$v_{\text{DC1}} = v_{\text{DC2}} = V_{\text{DC}} \tag{7}$$

Combining (3) ~ (7), the calculation of the SoC can be rewritten as

$$SoC_1 = SoC_1^* - \frac{1}{C_e V_{\text{DC}}}\int p_{\text{AC1}} dt \tag{8}$$

$$SoC_2 = SoC_2^* - \frac{1}{C_e V_{\text{DC}}}\int p_{\text{AC2}} dt \tag{9}$$

Perturbing (8) ~ (9) and transferring the results into s domain, it is reached that

$$s \cdot \hat{SoC}_1 = -\hat{p}_{\text{AC1}} / (C_e V_{\text{DC}}) \tag{10}$$

$$s \cdot \hat{SoC}_2 = -\hat{p}_{\text{AC2}} / (C_e V_{\text{DC}}) \tag{11}$$

where ^ denotes the perturbed values.

Take the two-order low-pass filter into account,

$$\text{L}(p_{\text{AC LPF1}}) = G_{\text{LPF}} \cdot \text{L}(p_{\text{AC1}}) \tag{12}$$

$$\text{L}(p_{\text{AC LPF2}}) = G_{\text{LPF}} \cdot \text{L}(p_{\text{AC2}}) \tag{13}$$

where L(·) denotes the Laplace transformation and G_{LPF} is shown as

$$G_{\text{LPF}} = \frac{\omega_0^2}{s^2 + 2\varsigma\omega_0 \cdot s + \omega_0^2} \tag{14}$$

where ω_0 is the cutting frequency and ς is the damped coefficient.

Perturbing (12) ~ (13) and substituting the results into (10) ~ (11), it is derived that

$$s \cdot \hat{SoC}_1 = -\hat{p}_{\text{AC LPF1}} / (C_e V_{\text{DC}} G_{\text{LPF}}) \tag{15}$$

$$s \cdot \hat{SoC}_2 = -\hat{p}_{\text{AC LPF2}} / (C_e V_{\text{DC}} G_{\text{LPF}}) \tag{16}$$

At the same time, employing SoC into the droop control method for active power sharing, (1) can be rewritten as

$$f_1 = f^* - (m_0 / SoC_1^{\text{n}}) \cdot p_{\text{AC LPF1}} \tag{17}$$

$$f_2 = f^* - (m_0 / SoC_2^{\text{n}}) \cdot p_{\text{AC LPF2}} \tag{18}$$

where m_0 is the initial droop coefficient when SoC equals to 1.

Perturbing (17) and (18), it is reached that

$$m_0 \cdot \hat{p}_{\text{AC LPF1}} = nSoC_1^{\text{n-1}}(F^* - F_1) \cdot \hat{SoC}_1 - SoC_1^{\text{n}} \cdot \hat{f}_1 \tag{19}$$

$$m_0 \cdot \hat{p}_{\text{AC LPF2}} = nSoC_2^{\text{n-1}}(F^* - F_2) \cdot \hat{SoC}_2 - SoC_2^{\text{n}} \cdot \hat{f}_2 \tag{20}$$

where ^ denotes the perturbed values and capital letters show the equilibrium point values.

Combining (15), (16), (19) and (20),

$$m_0 \hat{p}_{\text{AC LPF1}} = -nSoC_1^{\text{n-1}}(F^* - F_1) \cdot \hat{p}_{\text{AC LPF1}} / (C_e V_{\text{DC}} \cdot sG_{\text{LPF}}) - SoC_1^{\text{n}} \hat{f}_1 \tag{21}$$

$$m_0 \hat{p}_{\text{AC LPF2}} = -nSoC_2^{\text{n-1}}(F^* - F_2) \cdot \hat{p}_{\text{AC LPF2}} / (C_e V_{\text{DC}} \cdot sG_{\text{LPF}}) - SoC_2^{\text{n}} \hat{f}_2 \tag{22}$$

For simplification of (21) and (22), it is supposed that

$$k_{\text{in1}} = nSoC_1^{\text{n-1}}(F^* - F_1) / (C_e V_{\text{DC}}) \tag{23}$$

$$k_{\text{in2}} = nSoC_2^{\text{n-1}}(F^* - F_2) / (C_e V_{\text{DC}}) \tag{24}$$

Meanwhile, at the PCC,

$$p_{\text{AC1}} + p_{\text{AC2}} = P_{\text{load}} \tag{25}$$

where P_{load} is the load power at the PCC.

The frequencies at the different points in a microgrid can be regarded as the same, so

$$f_1 = f_2 \tag{26}$$

Perturbing (25) ~ (26) and transferring the results into s domain, together with (21) ~ (24), the characteristic equation of the SoC-based droop control system is achieved as

$$A \cdot s^2 + B \cdot s + C = 0 \tag{27}$$

where A, B and C are

$$A = k_{in1} SoC_2^n + k_{in2} SoC_1^n$$

$$B = 2\varsigma\omega_0 (k_{in1} SoC_2^n + k_{in2} SoC_1^n) + \omega_0^2 m_0 (SoC_1^n + SoC_2^n)$$

$$C = \omega_0^2 (k_{in1} SoC_2^n + k_{in2} SoC_1^n)$$

When the SoC of each energy storage unit and the power exponent n are changing, the dominant poles of the system are shown in Fig. 2 and 3. Here, the system parameters adopted are shown in Table I.

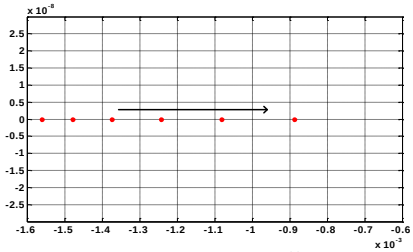

Fig. 2. Dominant poles with different SoC.

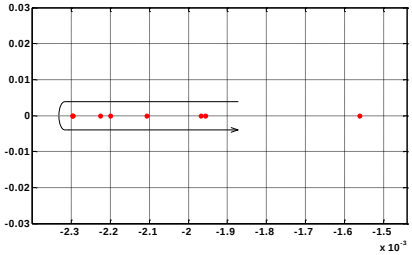

Fig. 3. Dominant poles with different power exponent n.

Combining (17), (18) and (26),

$$p_{AC\,LPF1} / p_{AC\,LPF2} = SoC_1^n / SoC_2^n \tag{28}$$

For the changing of SoC is much slower than that of the output active power, it can be supposed that

$$p_{AC1} / p_{AC2} \approx p_{AC\,LPF1} / p_{AC\,LPF2} = SoC_1^n / SoC_2^n \tag{29}$$

Combining (8) ~ (9), (25) and (29), it can be got that

$$SoC_1 = SoC_1^* - \frac{P_{load}}{C_e V_{DC}} \int \frac{SoC_1^n}{SoC_1^n + SoC_2^n} \mathrm{dt} \tag{30}$$

$$SoC_2 = SoC_2^* - \frac{P_{load}}{C_e V_{DC}} \int \frac{SoC_2^n}{SoC_1^n + SoC_2^n} \mathrm{dt} \tag{31}$$

The numeric solutions of (31) and (32) are reached with the parameters in Table I, as shown in Fig. 4. It is seen that with larger power exponent n, the active power sharing speed is much faster, as represented by the decreasing speed of SoC.

It should be noticed that the conventional droop method for equal reactive power sharing is adopted. For space limitation, more analyses will be shown in the final paper.

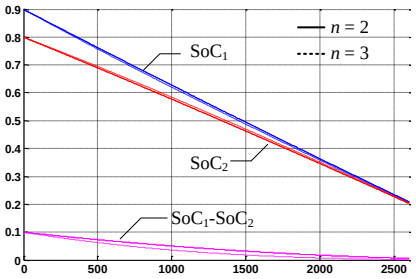

Fig. 4. Decreasing speed of SoC with different power exponent n.

TABLE I
SYSTEM PARAMETERS

Item	Symbol	Nominal Value	Unit
Initial SoC_1	SoC_1^*	90	%
Initial SoC_2	SoC_2^*	80	%
Initial Droop Coefficient	m_0	0.0006	V/kW
Load Resistance	R_{load}	20	Ω
Load Inductance	L_{load}	20	mH
Line Inductance	L_1 (L_2)	1.8	mH
Battery Capacity	C_e	600	Ah
Converter Input Voltage	V_{in}	600	V
AC Ref. Voltage (rms)	V_{AC}^*	230	V
AC Frequency	f_1(f_2)	50	Hz
LPF Cutting Frequency	ω_0	126	rads^{-1}
LPF Damping Ratio	ς	0.707	1
Switching Frequency	f_s	8	kHz

B. PCC voltage enhanced method for SoC-based droop control

In the conventional droop control method, the constant droop coefficients are employed in the control system. In this situation, the secondary control is employed to restore the deviation caused by the droop method. In the SoC-based droop control, the droop coefficients are adjusting according to the SoC of each energy storage unit. The applicability of secondary control should be further studied.

For the active power sharing, the secondary control diagram is shown in Fig. 5. In Fig. 5, ω_{MG} is the angular frequency at the PCC, ω^* and ω are the reference and actual values of the local frequency, G_{PI} is the secondary controller. For secondary control has remarkable characteristics of low-bandwidth communication, G_D is involved for modeling the communication delay. Here, the communication delay is set to 0.02s. It should be noticed that the squared part in Fig. 5 is used for the synchronization of the local output voltage and the PCC output voltage, which is adopted when the local converter begins to connect to the common bus. The transfer function of the control system is shown in (32).

$$\omega_{MG} = \frac{G_{PI} G_D G_{PLL}}{1 + G_{PI} G_D G_{PLL}} \cdot \omega_{MG}^* + \frac{G_{PLL}}{1 + G_{PI} G_D G_{PLL}} \cdot \omega^* - \frac{(1/SoC^n) \cdot G_{LPF} G_{PLL}}{1 + G_{PI} G_D G_{PLL}} \cdot p_{AC} \tag{32}$$

G_{PLL} represents the transfer function of the synchronization part, which is shown as

$$G_{PLL} = \frac{\tau}{\tau + s} \tag{33}$$

where τ is the time constant.

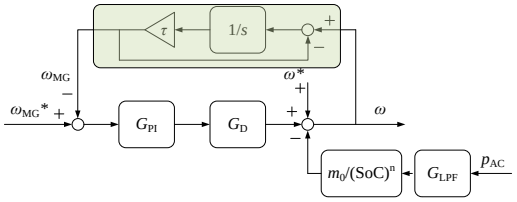

Fig. 5. Secondary control diagram for PCC voltage frequency restoration.

To show the stability of the system with different power exponent n and SoC, the corresponding bode plots are shown in Fig. 6. It can be seen that the stability of the PCC frequency restoration method for SoC-based droop control is guaranteed. It should be noticed that the transfer function from different inputs in (32) to ω_{MG} can be reached and the corresponding system stability can be guaranteed by the frequency analysis. For space limitation, more results will be shown in the final paper.

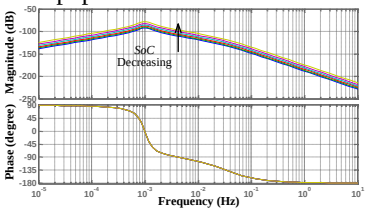

(a)

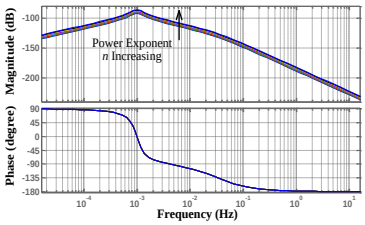

(b)

Fig. 6. Bode diagram for the transfer function from ω_{MG} to p_{AC}. (a) With changing SoC. (b) With changing power exponent n.

For the reactive power sharing, the secondary control diagram is shown in Fig. 7. The coefficient λ is involved to represent the ratio between the local voltage amplitude and PCC voltage amplitude. The derivation of the above ratio is shown below.

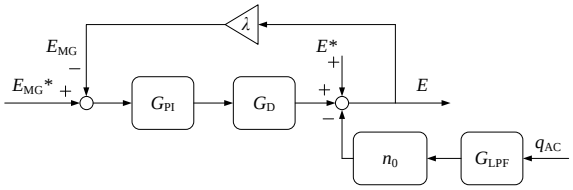

Fig. 7. Control diagram of secondary control for the PCC voltage amplitude restoration.

The parallel inverter system is simplified in Fig. 8. It is reached that

$$\frac{\dot{E}_1-\dot{E}_{MG}}{j\omega L_1}+\frac{\dot{E}_2-\dot{E}_{MG}}{j\omega L_2}=\frac{\dot{E}_{MG}}{R_{load}}+\frac{\dot{E}_{MG}}{j\omega L_{load}} \tag{34}$$

Therefore,

$$\lambda=\frac{E_{MG}}{E}=\frac{\left|\frac{1}{L_1}+\frac{1}{L_2}\right|}{\left|\frac{\omega}{R_{load}}-j(\frac{1}{L_1}+\frac{1}{L_2}+\frac{1}{L_{load}})\right|} \tag{35}$$

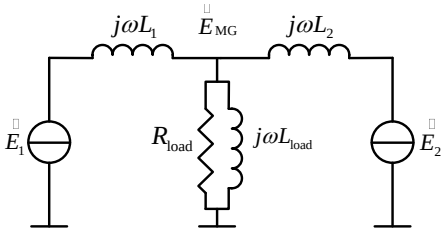

Fig. 8. Simplified model of the parallel inverter system.

It is seen from (35) that λ is in relation to the system frequency, while it can be demonstrated that even when ω is changing from $2\pi\cdot40$ rad/s to $2\pi\cdot60$ rad/s, λ changes slightly, with the maximum change less than 0.0001. According to the parameters shown in Table I, λ is selected as 0.9569. As same as the derivation for active power sharing, the transfer function for the control diagram in Fig. 7 is reached as

$$E_{MG}=\frac{\lambda G_{PI}G_D}{1+\lambda G_{PI}G_D}\cdot E^*_{MG}+\frac{\lambda}{1+\lambda G_{PI}G_D}\cdot E^* -\frac{\lambda n_q G_{LPF}}{1+\lambda G_{PI}G_D}\cdot q_{AC} \tag{36}$$

The bode plot from E_{MG} to each input variable in (36) can be reached. Take E_{MG} to E_{MG}^* as an example. The frequency domain analysis result is shown in Fig. 9. It is found that the system stability is guaranteed. More frequency domain analysis results will be shown in the final paper.

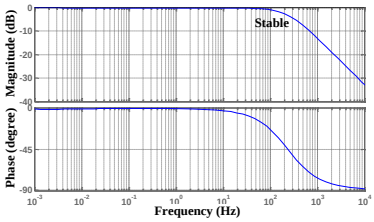

(a)

Fig. 9. Bode diagram for the transfer function from E_{MG} to E_{MG}^*.

III. Simulation and Experimental Validation

Matlab / Simulink model is accomplished to test the SoC-based droop control method with AC-bus voltage restoration function. The system parameters are also shown in Table I. The local AC voltage and current waveforms are shown in Fig. 10 and 11. It is seen that the local voltage and current waveforms have sinusoidal shape. With different power exponents, the active power sharing waveforms are shown in Fig. 12 ~ 14. It should be noticed that the constant time period is used in the simulation for comparison of the sharing effect with different n. It can be seen from Fig. 12 ~ 14 that with higher power exponent n, the active power sharing speed is faster. With the secondary control for PCC voltage, the frequency keeps stable at 50Hz, as shown in the magenta curve in Fig. 12 ~ 14. Meanwhile, equal reactive power sharing is guaranteed by droop control and the sharing error is controlled to be less than 30 Var. More results will be shown in the final paper.

The effect of secondary control in the above control diagram is shown in Fig. 15 and 16. It is seen that with secondary control, the frequency of the AC-bus voltage is

restored by 0.1 Hz and the amplitude of the AC-bus voltage is restored by 44.9V.

A 2×2.2 kW prototype with the control system of dSPACE 1103 is implemented to achieve the experimental test of the overall control system, as shown in Fig. 17. Here, for safety reason, the output power is lowered down, compared to the simulation results. As same as that in simulation, the local AC voltage and current waveforms are shown in Fig. 18 and 19. It is seen that the voltage and current waveforms have sinusoidal shape. With different power exponent *n*, the active power sharing waveforms are shown in Fig. 20 ~ 22. It can be seen that with larger *n*, the active power sharing speed is faster. Meanwhile, equal reactive power sharing is guaranteed by droop control and the sharing error is controlled to be less than 30 Var. More experimental results will be shown in the final paper.

The effect of secondary control is shown in Fig. 23 and 24. It is seen that the frequency of the PCC voltage is restored by 0.06 Hz and the amplitude of the PCC voltage is restored by 12 V.

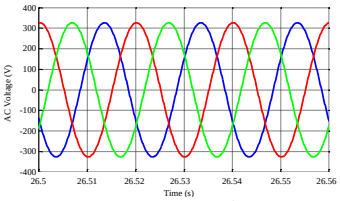

Fig. 10. Local AC voltage waveform (Simulation).

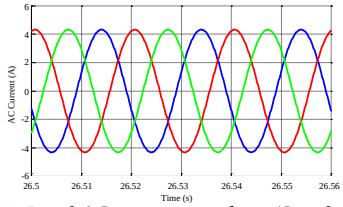

Fig. 11. Local AC current waveform (Simulation).

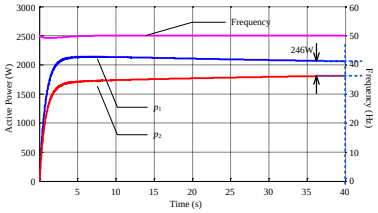

Fig. 12. Active power sharing waveform when n=2 (Simulation).

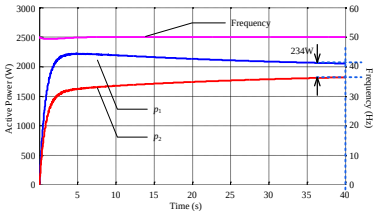

Fig. 13. Active power sharing waveform when n=3 (Simulation).

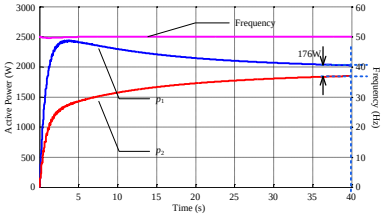

Fig. 14. Active power sharing waveform when n=6 (Simulation).

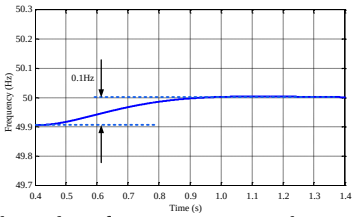

Fig. 15. AC-bus voltage frequency restoration by secondary control (Simulation).

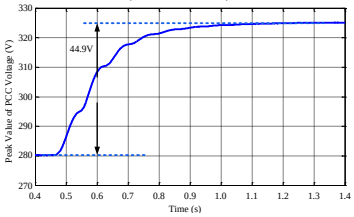

Fig. 16. AC-bus voltage amplitude restoration by secondary control (Simulation).

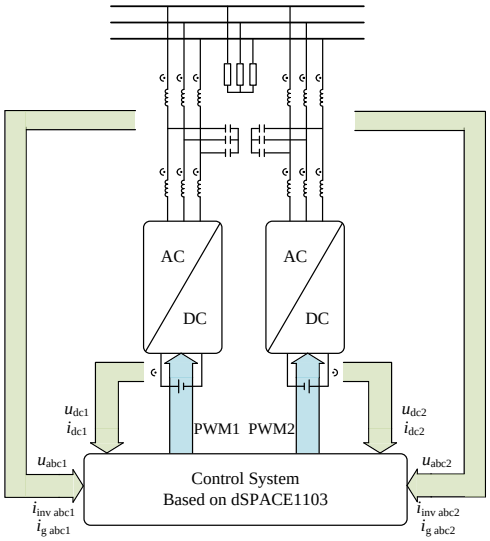

Fig. 17. Prototype structure.

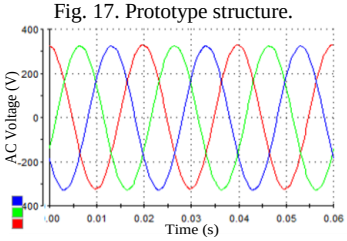

Fig. 18. Local AC voltage waveform (Experiment).

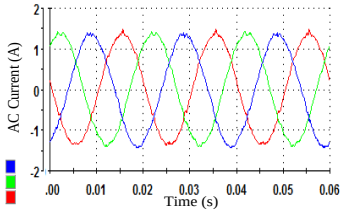

Fig. 19. Local AC current waveform (Experiment).

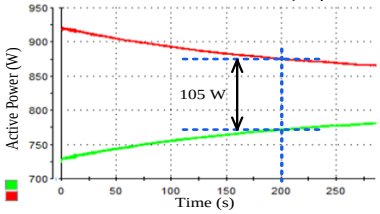

Fig. 20. Active power sharing waveform when n=2 (Experiment).

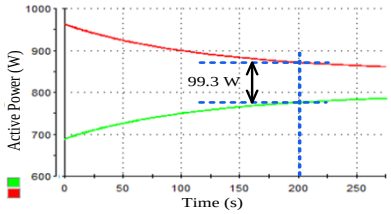

Fig. 21. Active power sharing waveform when n=3 (Experiment).

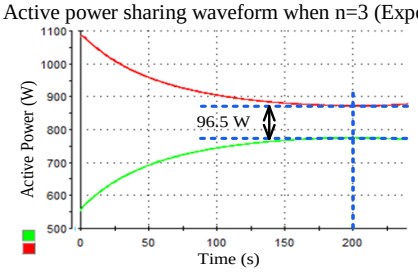

Fig. 22. Active power sharing waveform when n=6 (Experiment).

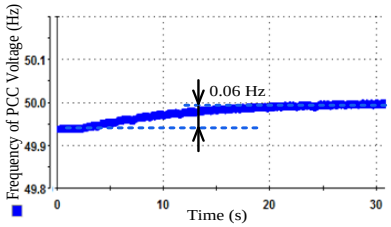

Fig. 23. AC-bus voltage frequency restoration by secondary control (Experiment).

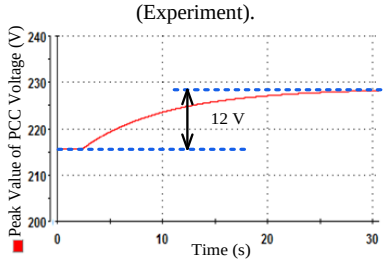

Fig. 24. AC-bus voltage amplitude restoration by secondary control (Experiment).

IV. Conclusion

To solve the power sharing problems in the distributed energy storage system in an AC microgrid, SoC-based droop control method with AC-bus voltage restoration is proposed.

1) By using SoC-based droop method, the energy storage unit with higher SoC generates more active power, and the one with lower SoC generates less. The droop coefficients for active power sharing are inversely proportional to SoC^n. Meanwhile, the conventional droop control for equal reactive power sharing is employed.

2) The dynamic performance of active power sharing is discussed. It is demonstrated that with larger power exponent *n*, the power sharing speed is faster. Small signal model of SoC-based droop control is developed and the system stability with changing SoC and different *n* is guaranteed.

3) In order to restore the deviation caused by the SoC-based droop control, secondary control is involved to restore the frequency and amplitude of the AC-bus voltage. Considering the changing SoC and different power exponents, the system model of secondary control is realized. The corresponding system stability of secondary control is tested.

The Matlab / Simulink simulation model and the 2×2.2 kW prototype were implemented. The theoretical analysis results are demonstrated by both simulation and experiment.

References

[1] R. Lasseter, A. Akhil, C. Marnay, J. Stevens, J. Dagle, etc, "The certs microgrid concept - white paper on integration of distributed energy resources," Technical report, U.S. Department of Energy, 2002.

[2] F. Blaabjerg, Z. Chen and S. B. Kjaer, "Power electronics as efficient interface in dispersed power generation systems," IEEE Trans. Power Electron., Vol. 19, No. 5, pp. 1184-1194, 2004.

[3] J.M. Guerrero, J. C. Vasquez, J. Matas, M. Castilla, etc, "Control strategy for flexible microgrid based on parallel line-interactive UPS systems," IEEE Trans. Ind. Electron., Vol. 56, No. 3, pp. 726-736, 2009.

[4] S. Luo, Z. Ye, R.L. Lin, F.C. Lee, "A classification and evaluation of paralleling methods for power supply modules," in Proc. IEEE PESC, 1999, pp. 901-908.

[5] J. M. Guerrero, J. C. Vasquez, J. Matas, etc, "Hierarchical control of droop-controlled AC and DC microgrids - a general approach toward standardization," IEEE Trans. Ind. Electron., Vol. 58, No. 1, pp. 158-172, 2011.

[6] H. Zhou, T. Bhattacharya, D. Tran, etc, "Composite energy storage system involving battery and ultracapacitor with dynamic energy management in microgrid applications," IEEE Trans. Power Electron., Vol. 26, No. 3, pp. 923-930, 2011.

[7] H. Kakigano, A. Nishino and T. Ise, "Distribution voltage control for DC microgrid with fuzzy control and gain-scheduling control," in Proc. of ECCE Asia, pp.256-263, 2011.

[8] Z. Ye, D. Boroyevich, K. Xing, F.C. Lee, "Design of parallel sources in DC distributed power systems by using gain-scheduling technique," in Proc. PESC, pp.161-165, 1999.